ELSEVIER

Chemical Engineering Journal 91 (2003) 167–174

Chemical Engineering Journal

www.elsevier.com/locate/cej

CFD modelling of continuous precipitation of barium sulphate in a stirred tank

Zdzisław Jaworski [a,b,*], Alvin W. Nienow [b]

[a] *Faculty of Chemical Engineering, Technical University of Szczecin, Aleja Piastow 42, 71-065 Szczecin, Poland*
[b] *School of Chemical Engineering, University of Birmingham, Birmingham, UK*

Abstract

By a combination of computational fluid dynamics (CFD), population balance and kinetic modelling, model solutions have been obtained for the precipitation of $BaSO_4$ in a dual-feed pipe, 0.3 m diameter continuous reactor agitated by a Rushton turbine. The conditions simulated include four agitator speeds from 200 to 950 rpm, two mean residence times (100 and 1180 s) and two shape factors ($k_v = 58$ and $\pi/6$). The flow field was solved using the multiple reference frame technique to give residuals $<10^{-4}$ and this solution was then transferred to a stationary reference frame and the iterations for other differential equations were carried out until the residuals were $<10^{-7}$. The results showed that >95% $BaSO_4$ precipitated in the reactor, which intuitively seems correct but this finding is in contrast to much lower values in earlier work, probably because of the more stringent convergence requirements used here. Agitation speed had little effect on the results, as has been recently shown in the literature, justifying the decision not to include a micromixing model in the analysis. However, mean residence time and shape factor did have a very substantial effect on the precipitate crystal size.

Keywords: Computational fluid dynamics (CFD); Modelling; Continuous precipitation; Stirred tank; Barium sulphate

1. Introduction

The precipitation reaction of barium chloride and sodium sulphate was used as a model reaction since it has been widely investigated experimentally and reported in the literature. In the last decade, modelling attempts have been made to simulate the precipitation process with the help of computational fluid dynamics (CFD) codes for simple precipitator geometries and for stirred tanks as well.

The first report of a successful CFD simulation of precipitation in a stirred tank was perhaps by Wei [1], followed by papers by Wei and Garside [2–4]. They used a CFD code for solving standard momentum and mass transport equations and added the moment equations for the crystal population balance. However, the simulated stirred tank was different from the one in which the data that were used for validation were obtained. In addition, the computational iterations were only continued until the normalised residuals fell just below 0.001. In other studies, e.g. [5], significant difficulties in obtaining fully converged CFD solutions for stirred tank precipitators were experienced. Hollander et al. [6] carried out a numerical scale-up study of agglomeration during calcium oxalate precipitation with assumed agglomeration kinetics. A simplified 2D flow simulation was also applied [7] to model gas–liquid precipitation system in a stirred tank and compared with results from other approaches and different mass transfer theories.

CFD studies in reactors of simpler geometry have been more successful. A jet mixing device [8], tubular reactors [9] as well as a rectangular flat reactor with jet mixing [10] were modelled. Generally, a significantly better agreement of the model predictions with the experimental data was found than for precipitation in stirred tanks. Recently, a successful application of the Fluent^{TM} 4.5 code was reported by Rousseaux et al. [11] to simulate the precipitation process of pseudo-boehmite in a sliding-surface mixing device, also with the moment equations for the crystal population balance. Three different modelling approaches, including CFD simulations, of Couette precipitators were utilised by Marchisio et al. [12]. They concluded that the modelling accuracy strongly depended on the quality of the CFD simulated flow field. Bałdyga and Orciuch [13] proposed a closure procedure based on the assumed beta probability density function and a satisfactory agreement was obtained in simulating turbulent precipitation of barium sulphate in tubular reactors.

Kinetic models of micromixing, nucleation, crystal growth and agglomeration, which are used in the CFD modelling of precipitation, are still being developed and

* Corresponding author. Tel.: +48-91-449-4020; fax: +48-91-449-4642.
E-mail address: jaworski@carbon.ps.pl (Z. Jaworski).

1385-8947/02/$ – see front matter
PII: S1385-8947(02)00150-X

Nomenclature

A, B	constants
cov	coefficient of size variation
C	species concentration (kmol/m^3)
Con	conversion ratio
G	crystal growth rate (m/s)
J	nucleation rate (number of crystals/m^3 s)
k_v	volumetric shape factor
K_{sp}	solubility product (kmol^2/m^6)
L_{43}	volume-based characteristic size (m)
m_j	jth moment of crystal size distribution (number of crystals m^j/m^3)
M	molecular mass (kg/kmol)
Res	numerical residuals
S	supersaturation ratio
S_{C_i}	source term (kg kmol/m^{6}s)
S_g	specific crystal growth rate (number of crystals kmol/m^4)
u	liquid velocity (m/s)
x	species mass fraction (kg/kg)

Greek symbols

γ	activity coefficient
Γ_{ef}	effective diffusion coefficient (m^2/s)
ρ	liquid density (kg/m^3)

refined. This development is needed mainly due to our limited empirical knowledge and fundamental understanding of those processes and the resulting implications for the numerical modelling of precipitators. For instance, there are contradictory reports on the influence of the impeller speed on the $BaSO_4$ crystal size in stirred precipitators, showing both a maximum [14,15] or a minimum [16]. For a calcium oxalate precipitation, weak effects of agitation in the continuous operation mode and moderate in the semi-batch were reported [17]. An experimental programme was performed [18] to investigate the errors introduced by the Reynolds averaging technique widely used in CFD and significant errors were found in the regions of high supersaturation and homogeneous nucleation. Other researchers [19,20] stressed the importance of non-homogeneous flow patterns on the local supersaturation and consequently on the local kinetics of precipitation. In addition, Aoun et al. [21] found that both the kinetics of nucleation and growth of barium sulphate crystals depends not only on the supersaturation ratio but also on the local excess of the reacting ions. Wong et al. [22] found the same parameters affecting mean particle size. A phenomenological model of macrodilution and coalescence-redispersion processes was used by Benet et al. [23], yielding predictions for barium sulphate precipitation in an impinging jet mixer very close to experimental results.

In stirred tanks, nucleation occurs mainly at the feeding point and according to Wijers et al. [24], the mesomixing time criterion should be used for scale-up. Taguchi et al. [25] found that macromixing was particularly important for stirred tank arrangements with micromixing being of lesser significance, which supports an earlier finding by Fitchett and Tarbell [14]. In a recent study, Wong et al. [22] also showed that, in the concentration range applied, impeller speed had a small effect on crystal size and morphology. Consideration of these results suggest that the contribution of mixing to the overall kinetics was marginal. Hence, micromixing effects have not been included in the modelling undertaken here. It may also be concluded that despite a large amount of experimental research on precipitation kinetics, further experiments are still required to clarify many of the mechanisms governing the many processes, which contribute to precipitation.

2. Precipitation model

The precipitation model used here was based on a set of the differential transport equations of momentum, chemical species and the crystal size distribution in moment form of the population balance for the $BaSO_4$ crystals with the boundary conditions for a model precipitator. Based on previous results for a tank with a single impeller [26], it can be expected that the macromixing process should be well simulated. However, the applied RANS modelling assumes homogeneity on the sub-grid scale and it implies that micromixing can be regarded as ideal. Accounting for a real, limited mixing intensity at the molecular scale has usually been reported in the literature to have been done by incorporating micromixing models. However, as discussed in the Introduction, micromixing effects have been neglected in the current modelling.

2.1. Precipitation reactor

A continuous flow stirred tank reactor (CSTR) with basic dimensions identical to those assumed by Wei and Garside [2] was modelled in this study. The cylindrical tank had a diameter of $T = 0.3$ m with a flat bottom and was filled with solutions up to $H = 0.3$ m. It was equipped with four standard baffles of width $T/10$ and a six-bladed Rushton turbine impeller of diameter $D = 0.10$ m, located at $H/2$. Four impeller speeds were applied, $N = 200$, 400, 600, 950 rpm. Two tubes were simulated each feeding a 0.1 M solution containing either $BaCl_2$ or Na_2SO_4. The modelling was always carried out with stoichiometric quantities of the two reactants being introduced to the precipitator. Thus, the feed rates of the two solutions were always equal and in the first part of this study were set to 18 ml/s. With the net working volume of 21.2 dm^3, the mean residence time, τ, was then about 20 min (1180 s). The same CSTR was also modelled in the second part of this study with a higher feeding rate, resulting in a shorter mean residence time of reactants of 100 s, which was identical to that in the reference study of

Wei and Garside [2]. The feed tubes were located at the free surface, on the opposite sides of the shaft, mid-way between two neighbouring baffles and roughly half way between the tank axis and wall. The reaction mixture exit was located in the centre of the tank bottom.

2.2. Model equations

The standard set of the Reynolds averaged Navier–Stokes equations, accompanied by the continuity equation and the standard k–ε turbulence model with wall functions were applied for momentum transfer. From the numerical solution of those equations the local values of the velocity vector components, u_j, and the turbulent viscosity, v_t, were obtained. The transport equations for all chemical entities, of molar concentration C_i (i = Ba, Cl, Na, SO_4, $BaSO_4$), were applied for the steady-state conditions. The equations had the general form of Eq. (1).

$$\mathrm{div}[puC_i + \Gamma_{\mathrm{ef}}\,\mathrm{grad}(pC_i)] = S_{C_i} \quad (1)$$

The source term, S_{C_i}, for the non-reacting ions (Cl, Na) was set to zero. For the other three entities, the source terms were set equal to the specific crystal growth rate, S_g, with (+) for $BaSO_4$ and with (−) for the Ba and SO_4 ions. This was equivalent to assuming that the crystal nucleation did not significantly contribute to the barium sulphate mass balance. The effective diffusivity, Γ_{ef}, was computed as a sum of the molecular diffusivity, D_m, and the turbulent, v_t/Sc_t. The turbulent Schmidt number, Sc_t, was assumed to be equal 0.7.

The specific crystal growth rate was related to the second moment of the crystal size distribution, m_2, and the volumetric crystal shape factor, k_v, Eq. (2). Two values of the shape factor were tested in the simulations, either $k_v = 348/6 = 58$ [27] for the long and short residence times or $k_v = \pi/6$ [8] for the short residence time.

$$S_g = (3m_2G)k_v\frac{\rho_{BaSO_4}}{M_{BaSO_4}} \quad (2)$$

The sensitivity to this parameter is very important as in practice a very wide range of shapes are formed [22].

Five crystal size distribution moments, from 0th to the 4th, were computed from the set of five equations of the crystal population balance [28], Eq. (3).

$$\mathrm{div}[um_j + \Gamma_{\mathrm{ef}}\,\mathrm{grad}(m_j)] = 0^j J + jm_{j-1}G \quad (j = 0\text{–}4) \quad (3)$$

The crystal growth rate, G, and the nucleation rate, J, were computed from the classical relations applied also by Wei and Garside [8] as functions of the local supersaturation ratio, S.

$$G = k_g(S-1)^2 \quad (4)$$

$$J = B\exp\left[-\frac{A}{\ln^2 S}\right] \quad (5)$$

The computations were performed assuming a temperature of 20 °C using $k_g = 4\times10^{-11}$ m/s, $B = 10^{36}$ number of crystals/m^3 s and $A = 2686$ for $S > 1000$ or $B = 146\times10^{10}$ number of crystals/m^3 s and $A = 67.3$ for $1 < S < 1000$. Local values of the supersaturation ratio were determined from local concentration of barium and sulphate ions, as well as from the other ion concentrations using the activity coefficient, γ, computed by the Bromley method [29].

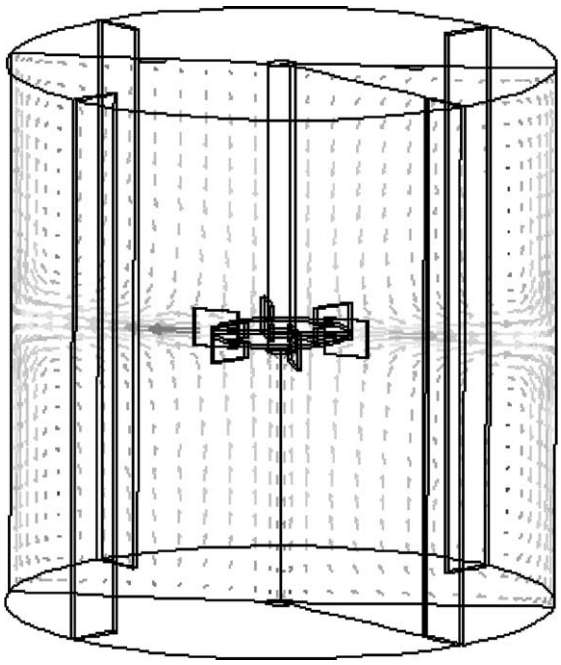

Fig. 1. Mean velocity vectors of the stirred liquid at $N = 200$ rpm.

$$S = \gamma\left(\frac{C_{Ba}C_{SO_4}}{K_{sp}}\right)^{0.5} \quad (6)$$

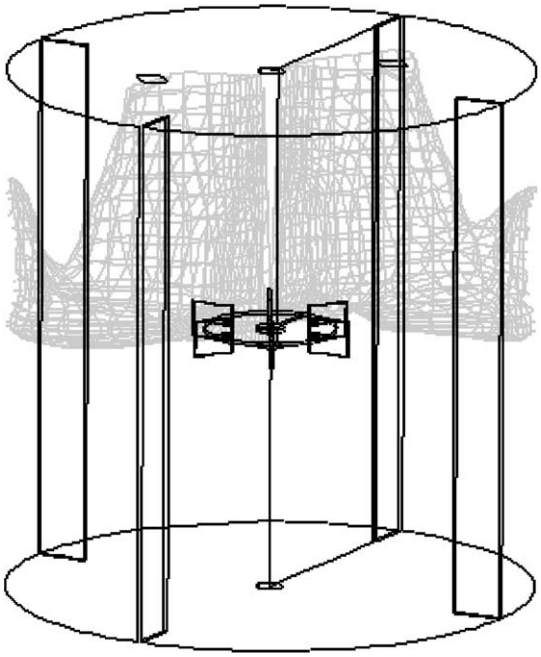

Fig. 2. Isosurface of $S = 40$ supersaturation for $N = 950$ rpm, short residence time.

The local ion concentrations were obtained from the iterative CFD solution of the transport Eq. (1). The value of the solubility product, K_{sp}, was also taken from [8] for the temperature of 20 °C as 1.1×10^{-10} kmol^2/m^6. The volume-based characteristic size of the crystals, L_{43}, was computed from the two crystal size distribution moments, m_4 and m_3.

$$L_{43} = \frac{m_4}{m_3} \tag{7}$$

Another factor characterising the crystal size distribution, which was analysed in this study was the coefficient of variation (cov).

$$\text{cov} = \left(\frac{m_2 m_0}{m_1^2} - 1 \right)^{0.5} \tag{8}$$

In addition, the conversion ratio of barium and sulphate ions into the solid form of barium sulphate in the exit stream (index "ex") from the precipitator was computed. The conversion (yield), Con_j, was defined as the ratio of the actually converted mass of the reacting species to the converted species mass for a condition of the chemical equilibrium.

$$\text{Con}_j = \frac{0.5(C_j)_{\text{in}} - (C_j)_{\text{ex}}}{0.5(C_j)_{\text{in}} - K_{\text{sp}}^{0.5}} \quad j = \text{Ba, SO}_4 \tag{9}$$

$$\text{Con}_{\text{BaSO}_4} = \frac{(C_{\text{BaSO}_4})_{\text{ex}}}{0.5(C_{\text{Ba}} + C_{\text{SO}_4})_{\text{in}} - K_{\text{sp}}^{0.5}} \tag{10}$$

The factor 0.5 in Eqs. (9) and (10) results from the presence of two inlet (index "in") streams to the precipitator.

2.3. Numerical solution

The CFD code used in this study was the structured Fluent^{TM} code, version 4.2 and a specialised preprocessor MixSim^{TM} for stirred tanks. The computational domain was

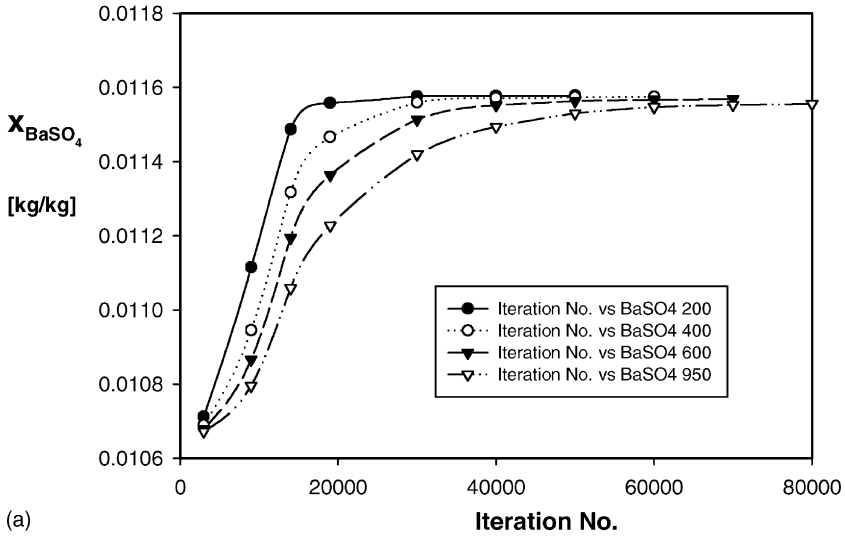

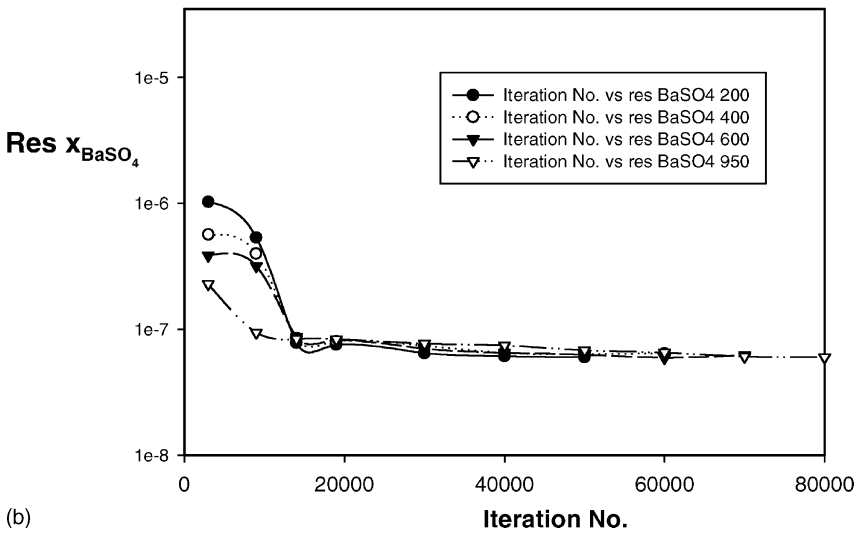

Fig. 3. (a) Effect of iteration number on the $BaSO_4$ mass fraction in the exit stream. (b) Normalised residuals for $BaSO_4$ at the precipitator exit.

divided into 56,448 control volumes by the numerical grid applied. The velocity (u) and turbulence fields were obtained in the first stage of these CFD simulations, assuming a liquid density and viscosity equal to those for water. The momentum transfer stage was done using the multiple reference frame option and a direct definition of the Rushton impeller geometry. After reaching convergence, with the sum of normalised residuals well below 10^{-4}, the solution was transferred to the stationary frame of reference and kept unchanged for the rest of the simulations. The same approach was used in earlier macromixing simulations (e.g. [26,30]).

An example of the mean velocity vectors in the vertical cross-section of the stirred precipitator is presented in Fig. 1, which shows a typical mean flow pattern for a Rushton turbine impeller in a baffled tank.

The simultaneous solution of five equations for the chemical entity, Eq. (1), and five equations of the crystal population balance, Eq. (3), were obtained in the second stage of these simulations. Instead of the molar concentration, C_i, the mass fraction, x_i, of the species was used when solving the transport equations. The convergence process of the numerical solution of the second stage was unstable in its initial phase and rather slow. It resulted in a relatively high number of iterations to satisfy the convergence criterion of normalised residuals lower than 10^{-7} (for the total reaction volume) and also to give a stable, final residual plateau for all concentration and moments. In order to obtain converged solutions efficiently for all species and moments required a special numerical strategy, which will be presented in a separate communication.

The required iteration number increased with increasing impeller speed, N, ranging from about 35,000 for 200 rpm to about 90,000 for 950 rpm. On average, each 10,000 iterations required about nine CPU hours on the

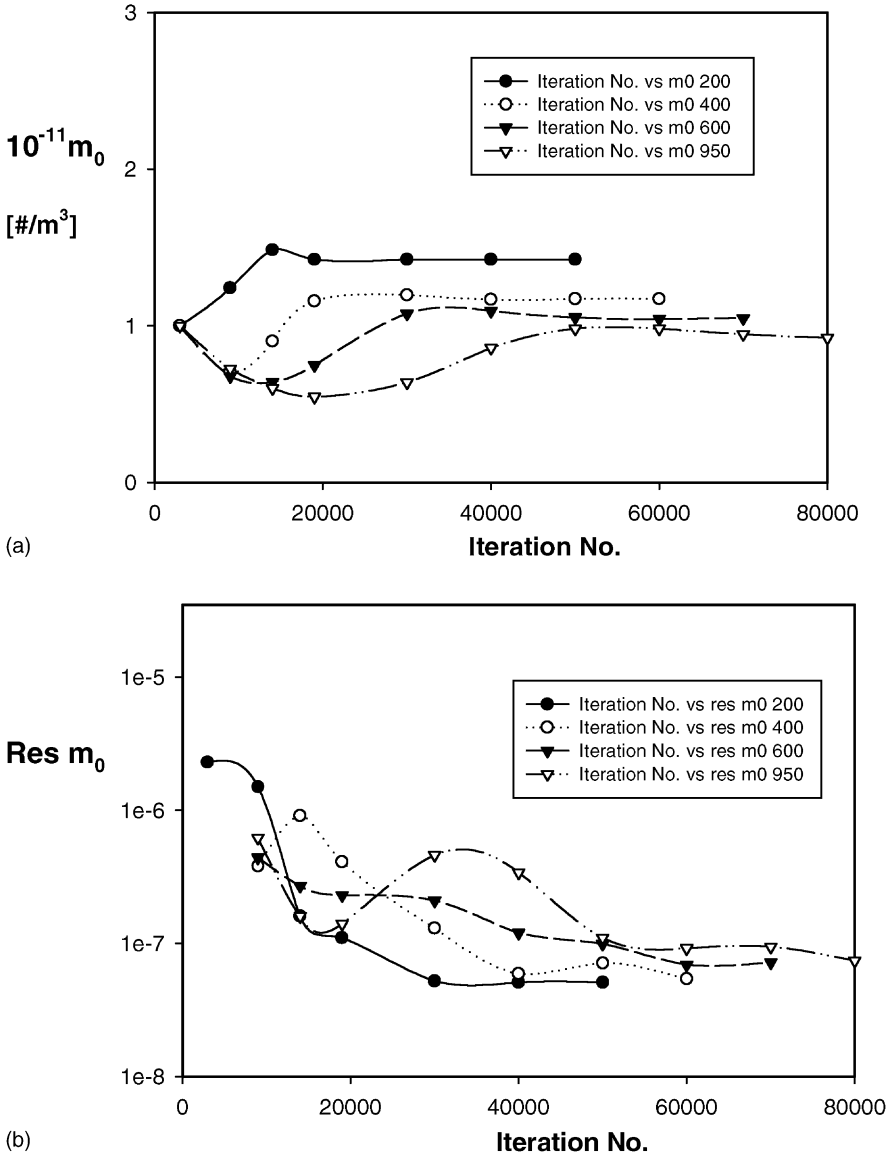

Fig. 4. (a) Effect of iteration number on the m_0 moment in the exit stream. (b) Normalised residuals for m_0 at the precipitator exit.

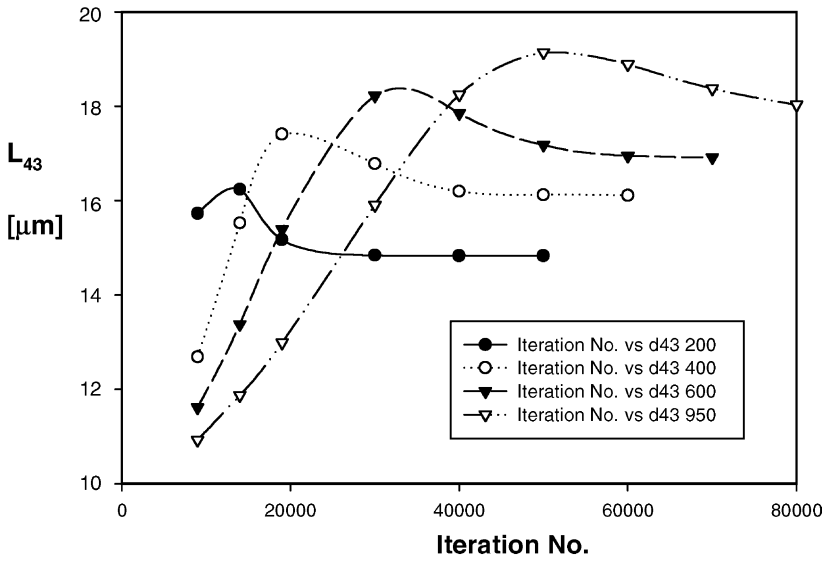

Fig. 5. Effect of iteration number on L_{43} in the exit stream.

computationally intensive Digital server. An example of the supersaturation distribution in the reaction volume is shown in Fig. 2 with maximum values close to the reactant inlets.

The completion of the convergence process was also controlled by monitoring the mass fraction, x_j, of the four ions and the precipitate in the exit stream from the precipitator. It was found that this was a more sensitive criterion of convergence than the stability of the residuals, Res x_j, for the five chemical species, cf. Fig. 3a and b. Similar plots for the 0th moment are shown in Fig. 4a and b for the four levels of the impeller speed applied in the simulations.

At the end of the iterations, the predicted L_{43} and the coefficient of size variation of the precipitate particles also reached steady, converged values as shown in Figs. 5 and 6.

3. Modelling results

The numerical results are presented in two sections, one for the case of the long residence time of the reactant streams and one for the short. The major results are given in tables to make easier a comparative analysis of the simulations.

3.1. Long residence time

The first case type considered was for the mean residence time of the reactants of 1180 s. Four levels of impeller speed, N, were used and only one value of the volume shape factor $k_v = 58$. The solution of the set of differential equations for momentum and mass transfer obtained, accompanied by the population balance equations, were further processed to

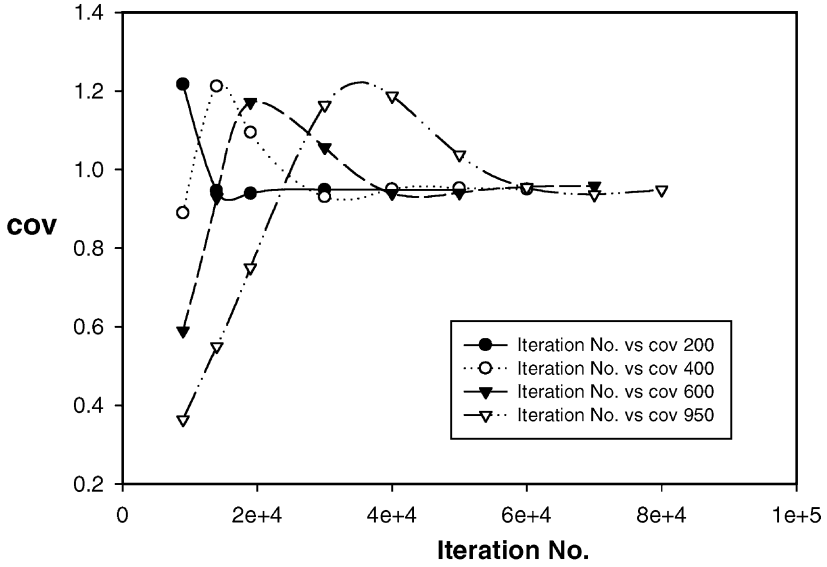

Fig. 6. Coefficient of size variation at the precipitator exit.

Table 1
Simulation results for the precipitator exit stream, long residence time

	Quantity			
	$N = 200$	$N = 400$	$N = 600$	$N = 950$
Con_{Ba}	0.99 (36)	0.99 (39)	0.99 (38)	0.99 (34)
Con_{SO_4}	0.99 (48)	0.99 (44)	0.99 (41)	0.99 (36)
Con_{BaSO_4}	0.99 (42)	0.99 (40)	0.99 (33)	0.99 (25)
$m_0 \times 10^{-11}$	1.424	1.173	1.052	0.920
$m_1 \times 10^{-6}$	0.557	0.497	0.465	0.426
$m_2 \times 10^{-1}$	0.414	0.401	0.393	0.381
$m_3 \times 10^{4}$	0.461	0.484	0.498	0.510
$m_4 \times 10^{9}$	0.683	0.789	0.842	0.911
L_{43} (μm)	14.8	16.1	16.9	17.9
cov	0.9 (49)	0.9 (51)	0.9 (55)	0.9 (65)

The values of N are in rpm.

Table 2
Simulation results for the precipitator exit stream, short residence time

	Quantity			
	$N = 200$[a]	$N = 950$[a]	$N = 200$[b]	$N = 950$[b]
Con_{Ba}	0.9843	0.9810	0.9564	0.9687
Con_{SO_4}	0.9892	0.9836	0.9704	0.9713
Con_{BaSO_4}	0.9881	0.9821	0.9631	0.9697
$m_0 \times 10^{-11}$	4.28	4.16	14.1	15.6
$m_1 \times 10^{-6}$	1.121	1.105	11.7	12.6
$m_2 \times 10^{-1}$	0.581	0.575	19.4	20.3
$m_3 \times 10^{4}$	0.450	0.448	48.5	49.0
$m_4 \times 10^{9}$	0.465	0.465	161	158
L_{43} (μm)	10.3	10.4	33.2	32.2
cov	1.10	0.986	0.999	0.997

The values of N are in rpm.
[a] $k_v = 348/6$.
[b] $k_v = \pi/6$.

provide information of direct process relevance. The data characterising the exit stream from the continuous flow precipitator is collected in Table 1.

From the data it follows that above 99% conversion of reactants into the crystal, solid form of $BaSO_4$ was obtained in the exit stream from the precipitator for all the impeller speeds used. Equivalent figures for the conversion of barium and of sulphate ions and for the formation of solid barium sulphate were between 99.2 and 99.5% for all the impeller speeds and can be regarded as essentially constant. However, such values were significantly higher than those estimated from Wei's results [1] (from ~0.40 to 0.85) for a residence time of 100 s, i.e. about 12 times shorter. Another estimate of the obtained crystal mass, based on the m_3 moment and the crystal shape factor of $k_v = 58$ (Bałdyga et al. [27]), resulted in values from 103% (200 rpm) to 114% (950 rpm) of the sum of the inlet mass flux of Ba and SO_4. It is believed that those values exceed the theoretical value of 100% mainly due to numerical errors and the applied model assumptions. Both ways of carrying out the mass balance were in fact rather similar and gave a value close to 100% as one would intuitively expect for a rapid process such as precipitation.

The volume averaged crystal size (L_{43}) in the exit stream converged in the range from 14 to 18 μm. These sizes are well in the range measured by Wong et al. [22] for two-pipe precipitation of $BaSO_4$. The precipitator crystal size moments, m_j, and the L_{43} characteristic size averaged over the whole reactor volume had only slightly smaller values than those in the exit stream. The simulation results in Table 1 suggest that the mean crystal size slowly increases with increasing impeller speed. Also the local concentrations and the supersaturation ratio, S, depended on the shape factor and for the considered cases the ratio changed from about 10 to 60. In a single simulated case, the local maximum and minimum S values differed inside the tank by a factor less than 5 with the maximum values close to the feed points. Such small differences were perhaps caused by a relatively crude numerical mesh. All coefficient of crystal size variation were only slightly different being close to 0.96. However, it should be stressed that the calculated values depend very much on the crystal shape factors used.

3.2. Short residence time

A similar simulation programme was repeated for the mean residence time of 100 s, as used in the Wei's study [1]. However, the simulations were performed for two different levels of the crystal shape factor, k_v, of either 58 or $\pi/6$, and the two extreme impeller speed levels, N, of either 200 or 950 rpm. The results for the precipitator exit stream are collected in Table 2.

For the higher value of the shape factor, the conversion percentage values were between 98.1 and 98.4% for the barium and sulphate ions as well as for the solid barium sulphate. On average, about 1% lower conversion was obtained compared to the long residence time cases with the same k_v value, but still much higher than the estimates from [1].

The simulations done for the small value of $k_v = \pi/6$ resulted in about three times larger particles in terms of the L_{43} dimension and a smaller conversion between 95.6 and 97.1%. Similarly, all the moments of the crystal size distribution computed were also the highest for $k_v = \pi/6$. Both the mean residence time and the crystal shape factor influenced the local supersaturation. The supersaturation values computed inside the precipitator for the impeller speed of 950 rpm gave values of 10–48 (for $\tau = 1180$ s, $k_v = 58$) or 16–110 (for $\tau = 100$ s, $k_v = 58$) or 34–151 (for $\tau = 100$ s, $k_v = \pi/6$).

4. Concluding remarks

The continuous precipitation of barium sulphate in a stirred tank reactor was successfully simulated by CFD and kinetic modelling. All the applied convergence criteria were satisfactorily fulfilled and the numerical solution strategy was of a great importance in doing so.

The computed level of conversion into solid barium sulphate was always higher than 95%. Such high values seem intuitively correct for rapid processes such as precipitation compared to the residence time in the reactor. These values are in marked contrast to previous CFD predictions for a dual-feed, continuous stirred precipitation reactor and can probably be attributed to the much lower level of residuals being used in order to satisfy the convergence requirements of the iteration process in this study. Both the residence time and the crystal shape factor significantly affected local supersaturation values inside the precipitator and the value of L_{43} for the crystals, but in all cases the coefficient of crystal size variation obtained was very close to the value of 1.0. In addition, agitator speed had little effect on crystal size.

There is still uncertainty regarding the role of micromixing and aggregation in the process of barium sulphate crystal growth and more experimental information is needed to clarify it. In addition, given the sensitivity of the predictions to the shape factor, much more information must be obtained on how this varies with operating parameters.

It is expected that the use of a finer grid around the feed points will improve accuracy of the numerical predictions of local supersaturation and kinetics of crystal nucleation and growth.

Acknowledgements

The financial support from EPSRC for ZJ, kind donation of the MixSim^{TM} software from Fluent^{TM} Europe plc as well the use of the computationally intensive server of the University of Birmingham are gratefully acknowledged.

References

[1] H. Wei, Application of computational fluid dynamics techniques to the modelling of precipitation processes, PhD Thesis, UMIST, 1997, UK.
[2] H. Wei, J. Garside, CFD-simulation of precipitation in stirred tanks, in: Proceedings of the IChemE Jubilee Research Event, Nottingham, UK, 1997, pp. 517–520.
[3] J. Garside, H. Wei, Pumped, stirred and maybe precipitated: simulation of precipitation process using CFD, Acta Polytechnica Scandinavica, Chem. Technol. 244 (1997) 9–15.
[4] H. Wei, J. Garside, Simulations and scale-up of precipitation processes using CFD techniques, in: Proceedings of the 3rd International Symposium on Mixing in Ind. Proc. ISMIP-3, Osaka, Japan, 1999, pp. 45–52.
[5] M.J.L. Van Leeuwen, Precipitation and mixing, PhD Thesis, Technical University Delft, Delft, Netherlands, 1998.
[6] E.D. Hollander, J.J. Derksen, O.S.L. Bruinsma, G.M. Van Rosmalen, H.E.A. Van den Akker, A numerical investigation into the influence of mixing on orthokinetic agglomeration, in: Proceedings of the 10th European Conference on Mixing, Delft, Netherlands, 2000, pp. 221–229.
[7] M.H. Al-Rashed, A.G. Jones, CFD modelling of gas-liquid reactive precipitation, Chem. Eng. Sci. 54 (21) (1999) 4779–4784.
[8] H. Wei, J. Garside, Application of CFD modelling to precipitation systems, Chem. Eng. Res. Des. 75 (A2) (1997) 219–227.
[9] J. Bałdyga, W. Orciuch, Closure problem for precipitation, Chem. Eng. Res. Des. 75 (A2) (1997) 160–170.
[10] M.L.J. Van Leeuwen, O.S.L. Bruinsma, G.M. Van Rosmalen, Influence of mixing on the product quality in precipitation, Chem. Eng. Sci. 51 (11) (1996) 2595–2600.
[11] J.M. Rousseaux, C. Vial, H. Muhr, E. Plasari, CFD simulation of precipitation in the sliding-surface mixing device, Chem. Eng. Sci. 56 (4) (2001) 1677–1685.
[12] D.L. Marchisio, A.A. Barresi, G. Baldi, Comparison of different modelling approaches to turbulent precipitation, in: Proceedings of the 10th European Conference on Mixing, Delft, Netherlands, 2000, pp. 77–84.
[13] J. Bałdyga, W. Orciuch, Closure problem for precipitation, Chem. Eng. Res. Des. 75 (A2) (1997) 160–170.
[14] D.E. Fitchett, J.M. Tarbell, Effect of mixing on the precipitation of barium sulphate in an MSMPR reactor, AIChE J. 36 (4) (1990) 511–522.
[15] W. Kim, J.M. Tarbell, Micromixing effects on barium sulphate precipitation in a double-jet semi batch reactor, Chem. Eng. Commun. 176 (1999) 89–113.
[16] J.F. Chen, C. Zheng, G.T. Chen, Interaction of macro- and micromixing on particle size distribution in reactive precipitation, Chem. Eng. Sci. 51 (10) (1996) 1957–1966.
[17] I. Houcine, E. Plasari, R. David, J. Villermaux, Influence of mixing characteristics on the quality and size of precipitated calcium oxalate in a pilot scale reactor, Chem. Eng. Res. Des. 75 (A2) (1997) 252–256.
[18] M.L.J. Van Leeuwen, O.S.L. Bruinsma, G.M. Van Rosmalen, Computational fluid dynamics approach to precipitation reactions: the importance of subgrid-scale fluctuations, in: Proceedings of the International Conference on Mixing and Crystal, Tioman Island, Malaysia, 2000, pp. 281–291.
[19] T. Manth, D. Mignon, H. Offermann, Experimental investigation of precipitation reactions under homogeneous mixing conditions, Chem. Eng. Sci. 51 (11) (1996) 2571–2576.
[20] T. Manth, D. Mignon, H. Offermann, The role of hydrodynamics in precipitation, J. Cryst. Growth 166 (1–4) (1996) 998–1003.
[21] M. Aoun, E. Plasari, R. David, J. Villermaux, Are barium sulphate kinetics sufficiently known for testing precipitation reactor models? Chem. Eng. Sci. 51 (10) (1996) 2449–2458.
[22] D.C.Y. Wong, Z. Jaworski, A.W. Nienow, Effect of ion excess on particle size and morphology during barium sulphate precipitation: an experimental study, Chem. Eng. Sci. 56 (3) (2001) 727–734.
[23] N. Benet, L. Falk, H. Muhr, E. Plasari, Characterisation and modelling of a two impinging jet mixer for precipitation processes using laser induced fluorescence, in: Proceedings of the 10th European Conference on Mixing, Delft, Netherlands, 2000, pp. 35–44.
[24] J.G. Wijers, J.H.A. Schoenmakers, D. Thoenes, Scaling-up of reactive crystallizers, in: Proceedings of the International Conference on Mixing and Crystal, Tioman Island, Malaysia, 2000, pp. 293–308.
[25] K. Taguchi, J. Garside, N.S. Tavare, Mixing, reaction and precipitation: semibatch barium sulphate precipitation, IChemE Symp. Ser. 146 (1999) 395–419.
[26] Z. Jaworski, J. Dudczak, CFD modelling of turbulent macromixing in stirred tanks. Effect of the probe size and number on mixing indices, Comp. Chem. Eng. 22 (1998) S293–S298.
[27] J. Bałdyga, W. Podgórska, R. Pohorecki, Mixing-precipitation model with application to double feed semibatch precipitation, Chem. Eng. Sci. 50 (8) (1995) 1281–1300.
[28] A.D. Randolph, M.A. Larson, Theory of Particulate Processes, 2nd Edition, Academic Press, New York, 1988.
[29] L.A. Bromley, Thermodynamic properties of strong electrolytes in aqueous solutions, AIChE J. 19 (2) (1973) 313–320.
[30] Z. Jaworski, W. Bujalski, N. Otomo, A.W. Nienow, CFD study of homogenization with dual Rushton turbines—comparison with experimental results. Part I. Initial studies, Trans. IChemE 78 (Part A) (2000) 327–333.